

# OPTIMISING DIFFERENT FEATURE TYPES FOR INPAINTING-BASED IMAGE REPRESENTATIONS

Ferdinand Jost      Vassilen Chizhov      Joachim Weickert \*

Mathematical Image Analysis Group, Faculty of Mathematics and Computer Science  
Campus E1.7, Saarland University, 66041 Saarbrücken, Germany  
{jost, chizhov, weickert}@mia.uni-saarland.de

## ABSTRACT

Inpainting-based image compression is a promising alternative to classical transform-based lossy codecs. Typically it stores a carefully selected subset of all pixel locations and their colour values. In the decoding phase the missing information is reconstructed by an inpainting process such as homogeneous diffusion inpainting. Optimising the stored data is the key for achieving good performance. A few heuristic approaches also advocate alternative feature types such as derivative data and construct dedicated inpainting concepts. However, one still lacks a general approach that allows to optimise and inpaint the data simultaneously w.r.t. a collection of different feature types, their locations, and their values. Our paper closes this gap. We introduce a generalised inpainting process that can handle arbitrary features which can be expressed as linear equality constraints. This includes e.g. colour values and derivatives of any order. We propose a fully automatic algorithm that aims at finding the optimal features from a given collection as well as their locations and their function values within a specified total feature density. Its performance is demonstrated with a novel set of features that also includes local averages. Our experiments show that it clearly outperforms the popular inpainting with optimised colour data with the same density.

**Index Terms**— Inpainting, Constrained Optimisation, Voronoi Diagram

## 1. INTRODUCTION

Inpainting is the process of reconstructing an image from a subset of its data [1]. One of its most challenging applications is lossy image compression. Inpainting-based codecs [2] typically store a few well chosen pixel locations of the original image with their greyscale or colour values. In the decoding phase, the missing image parts are inpainted from these sparse data, often with a diffusion process. These methods have been able to outperform even widely used transform-based codecs such as JPEG and JPEG2000 [3]. Surprisingly, already the simple linear process such as homogeneous diffusion inpainting can give good results, if the inpainting data is thoroughly optimised [4]. This, however, is a highly nontrivial problem.

For achieving better visual quality, it has also been advocated to replace the greyscale/colour data by gradient data [5, 6]. However, these papers had to undertake various specific algorithmic adaptations, and the data optimisation problem becomes even harder. To further improve the quality, it has been suggested to combine the gradient information with greyscale/colour data [6]. While this sounds

promising, it has not been done so far. Moreover, it would be desirable to have a more general framework that allows a straightforward incorporation of various classes of features without the need for dedicated optimisation algorithms.

### 1.1. Our Contributions

The goal of our paper is to address these challenges. Our contributions are threefold:

1. We establish a generalised inpainting framework for linear inpainting operators that can handle any collection of features in terms of linear equality constraints. This class is very large and includes e.g. derivatives of any order.
2. We introduce an efficient data selection strategy. It automatically distributes the available data budget among all different features and optimises both their locations and their values. This automates and generalises the otherwise cumbersome feature-specific selection and optimisation process.
3. We identify a novel collection of features that includes local averages. Experiments show that it considerably improves the inpainting quality compared to classical inpainting.

Since our paper focuses on feature integration and data optimisation, we postpone any coding aspects to future work.

### 1.2. Related Work

Some inpainting-based codecs involve information at edges [7, 8] or isolines [9]. However, these approaches still use grey values as their only feature and just benefit from the fact that contours allow an inexpensive encoding of their locations.

Extensions of edge-like concepts that combine greyscale data with the additional feature of discontinuities are presented in [10–12]. In contrast to our approach they use specific segmentation concepts which do not generalise to other feature classes.

There are various attempts to reconstruct an image from features such as zero-crossings [13] or topoints in scale-space [14], as well as junctions [15], and SIFT features [16]. While these papers give interesting information-theoretic insights, they do not offer competitive image representations in terms of compression quality.

Typically, an optimal placement of the features is crucial for the reconstruction quality. There has been a lot of work on spatial optimisation in the context of image inpainting, including analytic approaches [17], non-smooth optimisation [18–20], neural networks [21], probabilistic sparsification [4], and densification algorithms [22, 23]. By combining the ideas of error maps [22] and Voronoi densification [23], our approach falls into the latter class, but is the first one to generalise it to large collections of feature types.

\*This work has received funding from the European Research Council (ERC) under the European Union’s Horizon 2020 research and innovation programme (grant agreement no. 741215, ERC Advanced Grant INCOVID).

### 1.3. Paper Structure

In Section 2 we review homogeneous diffusion inpainting, we rewrite it as a constrained optimisation problem that covers many feature types, and we discuss efficient solution strategies for our novel, more general formulation. Section 3 introduces our strategy for optimising the feature locations and their values. Finally, we evaluate the performance of our framework in Section 4, and we give a conclusion and an outlook on future work in Section 5.

## 2. OUR FRAMEWORK

In this section we give an overview of classical sparse inpainting with homogeneous diffusion and rewrite it in a variational formulation. This allows us to extend the problem and introduce any set of features that can be formulated as linear equations. We then suggest an efficient solution strategy for this generalised inpainting problem.

### 2.1. Continuous Formulation

Consider a continuous greyscale image  $f(\mathbf{x}) : \Omega \rightarrow \mathbb{R}$  where  $\mathbf{x} := [x, y]^\top$  denotes a position in the rectangular image domain  $\Omega \subset \mathbb{R}^2$ . We assume that we have stored a sparse representation of  $f$  only on the set of the *inpainting mask*  $K \subset \Omega$ . A classical way [7] to inpaint the missing data is to compute a reconstruction  $u : \Omega \rightarrow \mathbb{R}$  by solving the Laplace equation with Dirichlet conditions on the mask  $K$  and reflecting boundary conditions on the domain boundary  $\partial\Omega$ :

$$\begin{aligned} -\Delta u(\mathbf{x}) &= 0, & \mathbf{x} \in \Omega \setminus K, \\ u(\mathbf{x}) &= f(\mathbf{x}), & \mathbf{x} \in K, \\ \partial_{\mathbf{n}} u(\mathbf{x}) &= 0, & \mathbf{x} \in \partial\Omega, \end{aligned} \quad (1)$$

where  $\Delta = \partial_{xx} + \partial_{yy}$  is the Laplacian, and  $\mathbf{n}$  denotes the normal vector to the boundary  $\partial\Omega$ . The fact that the Laplace equation  $\Delta u = 0$  is the steady state of the homogeneous diffusion equation  $\partial_t u = \Delta u$  [24] motivates the name *homogeneous diffusion inpainting*. Problem (1) can be derived as the Euler-Lagrange equation of the variational formulation

$$\begin{aligned} \min_u \frac{1}{2} \int_{\Omega} \|\nabla u(\mathbf{x})\|^2 d\mathbf{x} &= \min_u \frac{1}{2} \int_{\Omega} u(\mathbf{x})(-\Delta)u(\mathbf{x}) d\mathbf{x}, \\ \text{such that } u(\mathbf{x}) &= f(\mathbf{x}), \mathbf{x} \in K, \end{aligned} \quad (2)$$

where  $\|\cdot\|$  denotes the Euclidean norm, and  $\nabla = [\partial_x, \partial_y]^\top$  is the nabla operator. Here we have used the divergence theorem and the reflecting boundary conditions. This formulation will provide a straightforward way to introduce other types of constraints.

### 2.2. Discrete Formulation

Digital images are typically represented on a regular pixel grid. Then the discrete analogue of  $f$  can be represented as a vector  $\mathbf{f}$  with dimension  $N$  equal to the number of pixels. Similarly, we get the reconstruction vector  $\mathbf{u} \in \mathbb{R}^N$ . We also define the inpainting mask vector  $\mathbf{c} \in \{0, 1\}^N$  and its diagonal matrix  $\mathbf{C} = \text{diag}(\mathbf{c})$ . This allows to discretise the Dirichlet constraints  $u(\mathbf{x}) = f(\mathbf{x})$  on  $K$  as  $\mathbf{C}\mathbf{u} = \mathbf{C}\mathbf{f}$ . Finally we obtain the matrix  $\mathbf{L} \in \mathbb{R}^{N \times N}$  from the standard 5-point stencil discretisation of the negated Laplacian ( $-\Delta u_{i,j} \approx (-u_{i,j+1} - u_{i+1,j} + 4u_{i,j} - u_{i-1,j} - u_{i,j-1})/h^2$ ) with reflecting boundary conditions. Putting everything together results in the discrete analogue to Equation (2):

$$\min_u \frac{1}{2} \mathbf{u}^\top \mathbf{L} \mathbf{u}, \quad \text{s.t. } \mathbf{C}\mathbf{u} = \mathbf{C}\mathbf{f}. \quad (3)$$

Since  $\mathbf{L}$  is a discretisation of  $-\Delta$ , it is a positive semidefinite matrix. Thus, the above is a special case of a quadratic programming problem with linear equality constraints [25]. If the mask is non-empty, Equation (3) can be shown to have a unique solution that matches the unique solution of a direct discretisation of (1); see also [8].

### 2.3. Generalised Discrete Formulation

Our goal is to extend the discrete inpainting in Equation (3) to not only consider grey values as constraints, but a collection of features that can be implemented through linear equality constraints. To this end, we replace the Dirichlet constraints  $\mathbf{C}\mathbf{u} = \mathbf{C}\mathbf{f}$  by  $m$  types of constraints of the form  $\mathbf{C}_i \mathbf{A}_i \mathbf{u} = \mathbf{C}_i \mathbf{A}_i \mathbf{f}$  with  $i \in \{1, \dots, m\}$ :

$$\begin{aligned} \min_u \frac{1}{2} \mathbf{u}^\top \mathbf{L} \mathbf{u}, \quad \text{s.t. } \mathbf{A} \mathbf{u} &= \mathbf{b} \\ \mathbf{A} := \begin{bmatrix} \mathbf{C}_1 \mathbf{A}_1 \\ \dots \\ \mathbf{C}_m \mathbf{A}_m \end{bmatrix}, \quad \mathbf{b} := \begin{bmatrix} \mathbf{C}_1 \mathbf{A}_1 \mathbf{f} \\ \dots \\ \mathbf{C}_m \mathbf{A}_m \mathbf{f} \end{bmatrix}. \end{aligned} \quad (4)$$

The matrices  $\mathbf{A}_i \in \mathbb{R}^{N \times N}$  describe convolutions with user-defined feature stencils. For example, we can implement Dirichlet constraints through  $\mathbf{A}_1 = \mathbf{I}$  with identity matrix  $\mathbf{I}$ . First-order derivative constraints can be modelled by  $\mathbf{A}_2 = \mathbf{D}_x$  and  $\mathbf{A}_3 = \mathbf{D}_y$  with forward difference matrices  $\mathbf{D}_x, \mathbf{D}_y$  that approximate  $\partial_x, \partial_y$ . Also local integral constraints can be included easily, since they are linear operators as well. We also note that the above formulation is rather general w.r.t. the discrete linear inpainting operator  $\mathbf{L}$ : It can be any symmetric positive semidefinite matrix, e.g. a discretisation of the biharmonic operator  $\Delta^2$ . Considering linear inpainting operators and linear constraints keeps our discussion simple and is not very limiting, since they can give good reconstructions, if the data is optimised carefully [4]. Extending this inpainting to colour images is straightforward: We can treat each channel separately.

### 2.4. Numerical Solution Strategy

The constrained optimisation problem (4) can be solved with a Lagrange multiplier approach [25]. This turns it into an unconstrained one by introducing an additional vector  $\boldsymbol{\lambda} \in \mathbb{R}^{mN}$  of unknowns:

$$\min_u \max_{\boldsymbol{\lambda}} \left[ \frac{1}{2} \mathbf{u}^\top \mathbf{L} \mathbf{u} + \boldsymbol{\lambda}^\top (\mathbf{A} \mathbf{u} - \mathbf{b}) \right]. \quad (5)$$

Setting the derivatives w.r.t.  $\mathbf{u}$  and  $\boldsymbol{\lambda}$  to zero gives the linear system

$$\begin{bmatrix} \mathbf{L} & \mathbf{A}^\top \\ \mathbf{A} & \mathbf{0} \end{bmatrix} \begin{bmatrix} \mathbf{u} \\ \boldsymbol{\lambda} \end{bmatrix} = \begin{bmatrix} \mathbf{0} \\ \mathbf{b} \end{bmatrix}. \quad (6)$$

Its system matrix is symmetric but indefinite. After evaluating a variety of solvers, our algorithm of choice is SYMMLQ [26]. Similar to the conjugate gradients solver [27] it can be derived from the Lanczos method. However, unlike conjugate gradients, it is able to handle indefinite matrices. In fact, it can even handle singular systems as long as those have a solution. This is useful in our setting, since it even allows for features that are linearly dependent.

## 3. DATA OPTIMISATION

In order to achieve a good reconstruction quality with small error  $\|\mathbf{u} - \mathbf{f}\|^2$ , one must optimise the feature masks  $\mathbf{C}_i$  and the stored feature values  $\mathbf{b}$  in Equation (4). Thus, let us now propose an efficient and generic *spatial optimisation* algorithm for the masks  $\mathbf{C}_i$ , as well as a *tonal optimisation* method for the feature values  $\mathbf{b}$ .

### 3.1. Spatial Optimisation

Our spatial optimisation algorithm combines error maps [22] and a Voronoi densification [23] approach to efficiently construct the inpainting masks  $C_1, \dots, C_m$  for the features  $A_1, \dots, A_m$ . Given a target number of mask points  $|K|$ , it incrementally constructs the masks in  $n$  iterations (requiring  $n$  inpaintings). In each iteration, it introduces  $\lfloor |K|/n \rfloor$  mask points. More iterations require a longer runtime, but offer a better quality.

We want to find good locations for the  $\lfloor |K|/n \rfloor$  mask points to be inserted, using a minimal number of inpaintings. To this end, we use the inpainting  $\mathbf{u}$  from the previous iteration, and we compute  $m$  error maps  $|A_i(\mathbf{u} - \mathbf{f})|^2 \in \mathbb{R}^N$ ,  $i \in \{1, \dots, m\}$ . The absolute value squared  $|\cdot|^2$  is taken pointwise (in the colour case this is the Euclidean norm over RGB vectors); see Fig. 1, column 2 for an illustration. This expression allows us to minimise the mean squared error (MSE). The multiplication of the signed error  $\mathbf{u} - \mathbf{f}$  with  $A_i$  serves to capture the feature-wise error.

A straightforward application of the above error maps would be to insert mask points at the locations of highest pointwise error. However, this does not yield the best possible results, as it does not reflect the reduction of the error in the neighbourhood of the inserted points. As a simple approximation to capture this effect locally, we partition the image with the Voronoi decomposition induced by the current set of mask points. Then we integrate the  $m$  error maps in each cell, which gives  $m$  error values. Each cell is assigned its highest integrated error and the corresponding feature type. We then insert one mask point per cell in the  $\lfloor |K|/n \rfloor$  cells with largest error. The points within each cell are of the feature type of that cell. They are inserted at the location of the highest pointwise error in that cell. For an illustration, see Figure 1.

### 3.2. Tonal Optimisation

After the spatial optimisation, we can also optimise the values  $\mathbf{b}$  at the mask points. Since (6) is a system of linear equations, the inpainting part  $\mathbf{u}$  of its solution can be written as  $\mathbf{u} = \mathbf{R}\mathbf{b}$  with some reconstruction matrix  $\mathbf{R}$ . Our tonal optimisation problem then reads

$$\min_{\mathbf{b}} \|\mathbf{u} - \mathbf{f}\|^2 = \min_{\mathbf{b}} \|\mathbf{R}\mathbf{b} - \mathbf{f}\|^2. \quad (7)$$

It generalises the classical tonal optimisation of grey values [4] to a tonal optimisation of various feature types. If we set the derivative w.r.t.  $\mathbf{b}$  to zero, we obtain the normal equations

$$\mathbf{R}^\top \mathbf{R} \mathbf{b} = \mathbf{R}^\top \mathbf{f}. \quad (8)$$

We solve these normal equations with the CGNR algorithm [27]. For efficiency purposes we do not explicitly compute  $\mathbf{R}$ , since it is a dense matrix. Instead we use SYMMLQ [26] to evaluate the matrix-vector products with  $\mathbf{R}$  and  $\mathbf{R}^\top$  in the CGNR algorithm.

## 4. EXPERIMENTS

We illustrate the qualitative benefit of our framework on two natural colour images of size  $512 \times 512$ : *elpaso* and *windmill* (photos by J. Weickert). Our proposed example features consist of colour values, forward differences in  $x$ - and  $y$ -direction, and local colour averages on  $2 \times 2$  and  $16 \times 16$  patches, respectively.

Figure 3 studies the influence of the number of feature types in a sparse representation with a combined mask density of 5%. The masks are optimised with 30 iterations of our proposed Voronoi densification. Increasing the variety of features – while keeping the

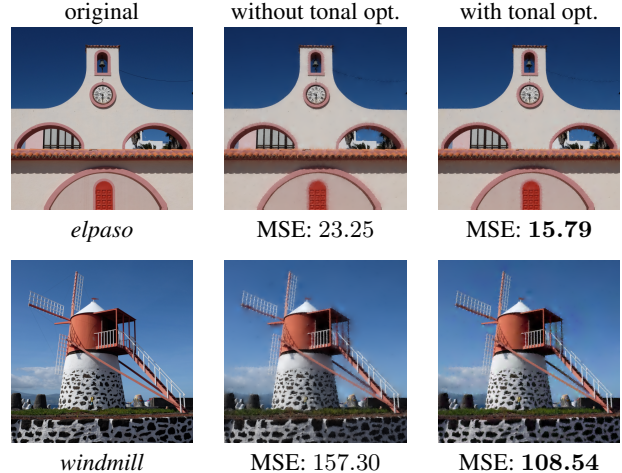


**Fig. 2:** Test images *elpaso* and *windmill* and their sparse representations using all five proposed feature types (total mask density: 5%) without and with tonal optimisation. The tonal optimisation improves the reconstruction quality by about one third.

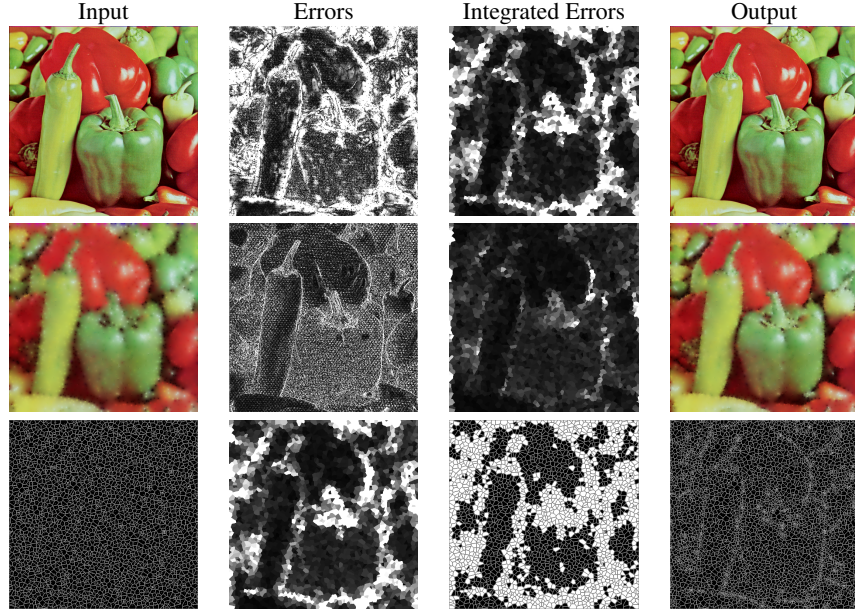
same total mask density – decreases the reconstruction error in a monotone way. This shows that all proposed feature types are beneficial, and that our optimisation strategy over the different feature types is effective in practice. It should be noted that using five feature types instead of a single one (the classical colour values) comes at basically no extra expense.

Figure 2 illustrates the impact of our generalised tonal optimisation. We observe that applying it to the spatially optimised representations with five feature types improves the MSE by about one third. Also here one should note that optimising the function values does not increase the total amount of data: Good values cost as much as bad ones.

## 5. CONCLUSIONS AND OUTLOOK

We have shown how an inpainting process can be generalised to incorporate an arbitrary set of different feature types in terms of linear constraints. While this problem appears to be fundamental, to our knowledge it has not been addressed in the inpainting community so far. In view of the simplicity and generality of its solution, this is surprising. On top of that, we have established the first generic approach for spatial and tonal optimisation for multiple different feature types. Finally we have demonstrated its practical relevance by the quality improvements with a novel set of features. The fact that multiscale local averages offer superior performance is another interesting observation that may deserve further attention in the future. These integrals form a natural complement to derivative features.

In our ongoing work, we are generalising our framework even further to nonlinear inpainting operators and constraints. Moreover, we also envision further improvements w.r.t. our data optimisation strategies and a wider range of feature types. Last but not least, we will integrate all these concepts in a practical codec that optimises not only for reconstruction quality but also for coding costs.



**Fig. 1:** Steps in a single iteration of our densification algorithm. The **first column** is the output of the previous step. From top to bottom: reference image, inpainting, mask with Voronoi diagram. The **second column** consists of the error maps for the Dirichlet and  $\partial_x$  features, and the maximum cell-wise integrated errors. The **third column** contains cell-wise integrated errors for the Dirichlet and  $\partial_x$  features, and the selected  $\lfloor |K|/n \rfloor$  cells with largest errors that are to be refined (in white). The **last column** shows the output of this iteration: reference image, new inpainting, and updated mask with Voronoi diagram.

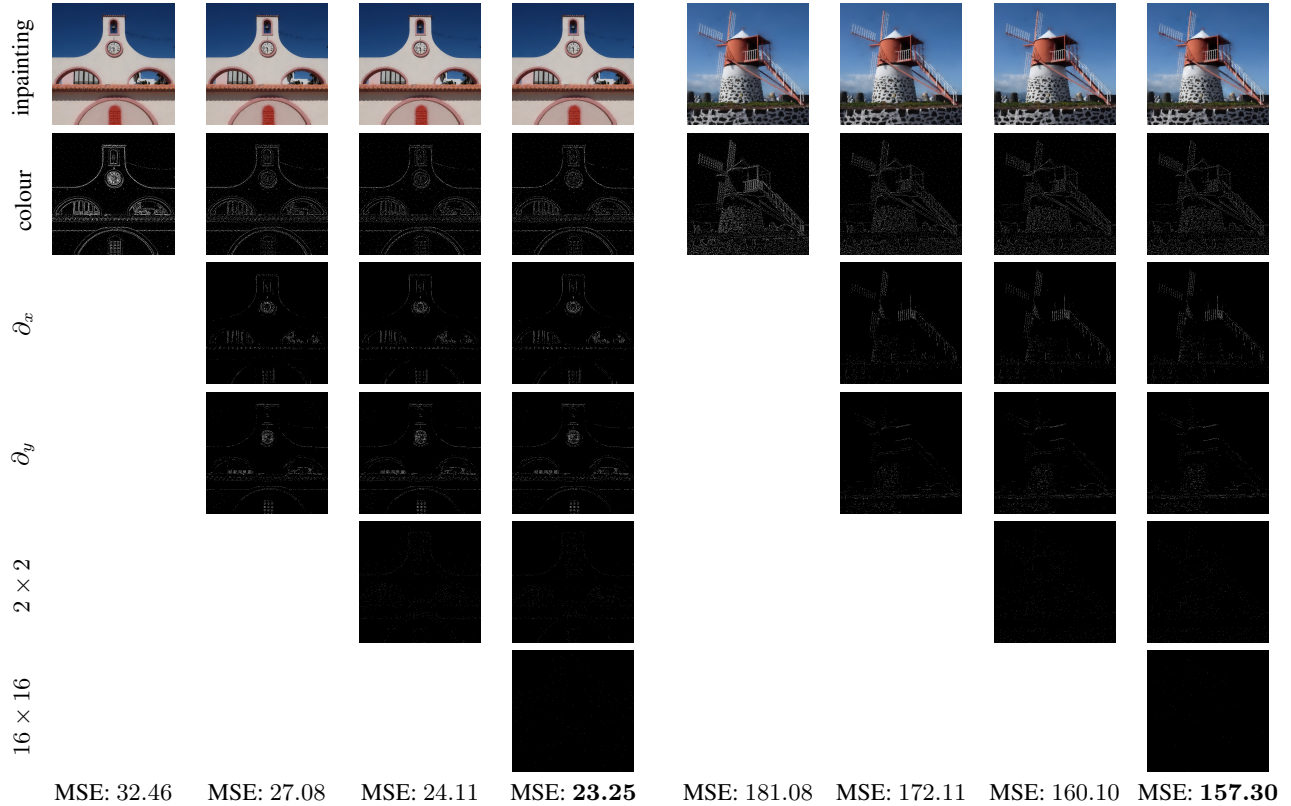


**Fig. 3:** Masks and inpainting results for *elpaso* and *windmill*. The combined mask density is 5%. All masks are generated with 30 iterations of our Voronoi densification. Each column gives masks and inpainting result for a different set of feature types. Increasing the variety of feature types improves the reconstruction quality without increasing the total amount of information.

## 6. REFERENCES

- [1] C. Guillemot and O. Le Meur, “Image inpainting: Overview and recent advances,” *IEEE Signal Processing Magazine*, vol. 31, no. 1, pp. 127–144, 2014.
- [2] I. Galić, J. Weickert, M. Welk, A. Bruhn, A. Belyaev, and H.-P. Seidel, “Towards PDE-based image compression,” in *Variational, Geometric and Level-Set Methods in Computer Vision*, N. Paragios, O. Faugeras, T. Chan, and C. Schnörr, Eds., vol. 3752 of *Lecture Notes in Computer Science*, pp. 37–48. Springer, Berlin, 2005.
- [3] C. Schmaltz, P. Peter, M. Mainberger, F. Ebel, J. Weickert, and A. Bruhn, “Understanding, optimising, and extending data compression with anisotropic diffusion,” *International Journal of Computer Vision*, vol. 108, no. 3, pp. 222–240, July 2014.
- [4] M. Mainberger, S. Hoffmann, J. Weickert, C. H. Tang, D. Johannsen, F. Neumann, and B. Doerr, “Optimising spatial and tonal data for homogeneous diffusion inpainting,” in *Scale Space and Variational Methods in Computer Vision*, A. M. Bruckstein, B. ter Haar Romeny, A. M. Bronstein, and M. M. Bronstein, Eds., vol. 6667 of *Lecture Notes in Computer Science*, pp. 26–37. Springer, Berlin, 2012.
- [5] E.-M. Brinkmann, M. Burger, and I. Grah, “Regularization with sparse vector fields: From image compression to TV-type reconstruction,” in *Scale Space and Variational Methods in Computer Vision*, J.-F. Aujol, M. Nikolova, and N. Papadakis, Eds., vol. 9087 of *Lecture Notes in Computer Science*, pp. 191–202. Springer, Berlin, 2015.
- [6] M. Schneider, P. Peter, S. Hoffmann, J. Weickert, and E. Meinhardt-Llopis, “Gradients versus grey values for sparse image reconstruction and inpainting-based compression,” in *Advanced Concepts for Intelligent Vision Systems*, J. Blanc-Talon, C. Distant, W. Philips, D. Popescu, and P. Scheunders, Eds., vol. 10016 of *Lecture Notes in Computer Science*, pp. 1–13. Springer, Cham, 2016.
- [7] S. Carlsson, “Sketch based coding of grey level images,” *Signal Processing*, vol. 15, pp. 57–83, 1988.
- [8] M. Mainberger, A. Bruhn, J. Weickert, and S. Forchhammer, “Edge-based compression of cartoon-like images with homogeneous diffusion,” *Pattern Recognition*, vol. 44, no. 9, pp. 1859–1873, Sept. 2011.
- [9] A. Solé, V. Caselles, G. Sapiro, and F. Arandiga, “Morse description and geometric encoding of digital elevation maps,” *IEEE Transactions on Image Processing*, vol. 13, no. 9, pp. 1245–1262, Sept. 2004.
- [10] S. Hoffmann, M. Mainberger, J. Weickert, and M. Puhl, “Compression of depth maps with segment-based homogeneous diffusion,” in *Scale Space and Variational Methods in Computer Vision*, A. Kuijper, K. Bredies, T. Pock, and H. Bischof, Eds., vol. 7893 of *Lecture Notes in Computer Science*, pp. 319–330. Springer, Berlin, 2013.
- [11] F. Jost, P. Peter, and J. Weickert, “Compressing flow fields with edge-aware homogeneous diffusion inpainting,” in *Proc. 2020 International Conference on Acoustics, Speech, and Signal Processing*, Barcelona, Spain, May 2020, pp. 2198–2202.
- [12] F. Jost, P. Peter, and J. Weickert, “Compressing piecewise smooth images with the Mumford–Shah cartoon model,” in *Proc. 28th European Signal Processing Conference*, Amsterdam, Netherlands, Jan. 2021, pp. 511–515.
- [13] Y. Zeevi and D. Rotem, “Image reconstruction from zero-crossings,” *IEEE Transactions on Acoustics, Speech, and Signal Processing*, vol. 34, pp. 1269–1277, 1986.
- [14] F. M. W. Kanters, M. Lillholm, R. Duits, B. J. P. Jansen, B. Platel, L. M. J. Florack, and B. M. ter Haar Romeny, “On image reconstruction from multiscale top points,” in *Scale Space and PDE Methods in Computer Vision*, R. Kimmel, N. Sochen, and J. Weickert, Eds., vol. 3459 of *Lecture Notes in Computer Science*, pp. 431–439. Springer, Berlin, 2005.
- [15] V. Caselles, B. Coll, and J.-M. Morel, “Junction detection and filtering,” in *Foundations of Computational Mathematics*, F. Cucker and M. Shub, Eds., pp. 23–42. Springer, Berlin, 1997.
- [16] P. Weinzaepfel, H. Jégou, and P. Pérez, “Reconstructing an image from its local descriptors,” in *Proc. 2011 IEEE Computer Society Conference on Computer Vision and Pattern Recognition*, Colorado Springs, CO, June 2011, pp. 337–344, IEEE Computer Society Press.
- [17] Z. Belhachmi, D. Bucur, B. Burgeth, and J. Weickert, “How to choose interpolation data in images,” *SIAM Journal on Applied Mathematics*, vol. 70, no. 1, pp. 333–352, 2009.
- [18] L. Hoeltgen, S. Setzer, and J. Weickert, “An optimal control approach to find sparse data for Laplace interpolation,” in *Energy Minimisation Methods in Computer Vision and Pattern Recognition*, A. Heyden, F. Kahl, C. Olsson, M. Oskarsson, and X.-C. Tai, Eds., vol. 8081 of *Lecture Notes in Computer Science*, pp. 151–164. Springer, Berlin, 2013.
- [19] P. Ochs, Y. Chen, T. Brox, and T. Pock, “iPiano: Inertial proximal algorithm for nonconvex optimization,” *SIAM Journal on Imaging Sciences*, vol. 7, pp. 1388–1419, 2014.
- [20] S. Bonettini, I. Loris, F. Porta, M. Prato, and S. Rebegoldi, “On the convergence of a linesearch based proximal-gradient method for nonconvex optimization,” *Inverse Problems*, vol. 33, no. 5, 2017, Article 055005.
- [21] T. Alt, P. Peter, and J. Weickert, “Learning sparse masks for diffusion-based image inpainting,” in *Pattern Recognition and Image Analysis*, A. J. Pinho, P. Georgieva, L. F. Teixeira, and J. A. Sánchez, Eds., Cham, 2022, vol. 13256 of *Lecture Notes in Computer Science*, pp. 528–539, Springer.
- [22] L. Karos, P. Bheed, P. Peter, and J. Weickert, “Optimising data for exemplar-based inpainting,” in *Advanced Concepts for Intelligent Vision Systems*, J. Blanc-Talon, D. Helbert, W. Philips, D. Popescu, and P. Scheunders, Eds., vol. 11182 of *Lecture Notes in Computer Science*, pp. 547–558. Springer, Berlin, Sept. 2018.
- [23] V. Daropoulos, M. Augustin, and J. Weickert, “Sparse inpainting with smoothed particle hydrodynamics,” *SIAM Journal on Imaging Sciences*, vol. 14, no. 4, pp. 1669–1705, 2021.
- [24] T. Iijima, “Basic theory on normalization of pattern (in case of typical one-dimensional pattern),” *Bulletin of the Electrotechnical Laboratory*, vol. 26, pp. 368–388, 1962, In Japanese.
- [25] P. E. Gill, W. Murray, and M. H. Wright, *Practical Optimization*, Academic Press, London, 1981.
- [26] C. C. Paige and M. A. Saunders, “Solution of sparse indefinite systems of linear equations,” *SIAM Journal on Numerical Analysis*, vol. 12, no. 4, pp. 617–629, 1975.
- [27] Y. Saad, *Iterative Methods for Sparse Linear Systems*, SIAM, Philadelphia, second edition, 2003.

## APPENDIX A. ADDITIONAL EXPERIMENTS

In our experimental evaluation we have used two images to illustrate the performance of our framework (see Figure 3). However, those results also generalise to other images, with slight deviations depending on the frequencies of the images. To validate this claim, we present additional experiments in Figure 4 on standard test images used in the signal processing literature. The dependence on the fre-



image	grey values	$\partial_x + \partial_y$	$2 \times 2$	$16 \times 16$
trui	38.45	38.51	32.53	31.99
cameraman	138.27	115.55	110.67	107.90
house	58.78	53.42	50.69	50.48
ballet	7.29	2.34	2.29	2.17

**Fig. 4:** Additional results for greyscale images *trui*, *cameraman*, *house* and depth map *ballet*. The table shows MSE values for an increasing number of feature types from left to right, similar to Figure 3. The combined density is again 5% with 30 iterations of our spatial optimisation algorithm.

quencies is an effect of the homogeneous diffusion inpainting, rather than the features and the specifics of our framework. The slight increase in MSE for *trui* using greyvalues and derivative features (the  $\partial_x + \partial_y$  column) is caused by inaccuracies of the MSE approximation used in our spatial optimisation stage (see Section 3.1). Namely, we use the error maps  $|\mathbf{A}_i(\mathbf{u} - \mathbf{f})|^2$  as predictors of the MSE in order to select mask point locations at a lower computational cost.

## APPENDIX B. TONAL OPTIMISATION

In section 3.2 we defined the reconstruction as  $\mathbf{u} = \mathbf{R}\mathbf{b}$  in order to formulate the tonal optimisation problem in a concise manner. Here we make the meaning of  $\mathbf{R} \in \mathbb{R}^{N^m \times N^m}$  and  $\mathbf{b} \in \mathbb{R}^{N^m}$  precise. The definition of  $\mathbf{R}$  can be derived starting from (6) as follows:

$$\begin{aligned} \begin{bmatrix} \mathbf{L} & \mathbf{A}^T \\ \mathbf{A} & \mathbf{0} \end{bmatrix} \begin{bmatrix} \mathbf{u} \\ \lambda \end{bmatrix} &= \begin{bmatrix} \mathbf{0} \\ \mathbf{b} \end{bmatrix} \\ \begin{bmatrix} \mathbf{u} \\ \lambda \end{bmatrix} &= \begin{bmatrix} \mathbf{L} & \mathbf{A}^T \\ \mathbf{A} & \mathbf{0} \end{bmatrix}^+ \begin{bmatrix} \mathbf{0} \\ \mathbf{I} \end{bmatrix} \mathbf{b} \\ \mathbf{u} = \mathbf{R}\mathbf{b} &= \begin{bmatrix} \mathbf{I} & \mathbf{0} \end{bmatrix} \begin{bmatrix} \mathbf{L} & \mathbf{A}^T \\ \mathbf{A} & \mathbf{0} \end{bmatrix}^+ \begin{bmatrix} \mathbf{0} \\ \mathbf{I} \end{bmatrix} \mathbf{b}. \end{aligned}$$

In the above  $M^+$  is the Moore-Penrose pseudoinverse of  $M$ . We do not compute it in practice, instead we solve Equation (6) using the SYMMLQ solver and keep only the  $\mathbf{u}$  part.

The vector  $\mathbf{b}$  can be any vector from  $\mathbb{R}^{N^m}$  (in the range of the system matrix) with zeroes at indices corresponding to non-mask pixels. That is, if the mask for the  $i$ -th feature  $\mathbf{C}_i$  does not have a mask pixel at index  $j$ , i.e.  $(\mathbf{C}_i)_{jj} = 0$ , then the value of  $\mathbf{b}$  at index  $iN + j$  is zero:  $b_{iN+j} = 0$ . The specific choice  $\mathbf{b} = \mathbf{A}\mathbf{f}$  in (4) interpolates  $\mathbf{f}$ 's grey/colour values, derivatives, and local integrals. However, we can theoretically store any values (i.e. not necessarily interpolating  $\mathbf{f}$ ) at mask points. The optimal ones in terms of the Euclidean distance minimise  $\|\mathbf{u} - \mathbf{f}\| = \|\mathbf{R}\mathbf{b} - \mathbf{f}\|$ . Tonal optimisation finds those optimal values.

## APPENDIX C. SYMMLQ SOLVER

To solve Equation (6) we use the SYMMLQ [26] solver. However, in the literature the algorithm is typically not given explicitly. For completeness we provide pseudocode for the solver in Alg. 1. Let  $\mathbf{M} \in \mathbb{R}^{n \times n}$  be a symmetric indefinite matrix (e.g. the matrix in (6)), let  $\mathbf{b}$  be in the range of  $\mathbf{M}$ , and we wish to solve  $\mathbf{M}\mathbf{x} = \mathbf{b}$ , given some initial guess  $\mathbf{x} \in \mathbb{R}^n$  (potentially the zero vector). We denote by  $\langle \mathbf{u}, \mathbf{v} \rangle = \sum_{i=1}^n u_i v_i$  the usual dot product, and by  $\|\mathbf{u}\| = \sqrt{\langle \mathbf{u}, \mathbf{u} \rangle}$  the induced norm. Note that in our implementation of (6), all matrix-vector products are performed in a matrix-free fashion in order to maximise efficiency.

### Algorithm 1: SYMMLQ Solver

---

```

Data:  $\epsilon > 0$ ,  $\mathbf{M} \in \mathbb{R}^{n \times n}$ ,  $\mathbf{b} \in \mathbb{R}^n$ ,  $\mathbf{x} \in \mathbb{R}^n$ 
Result:  $\mathbf{x} \in \mathbb{R}^n : \mathbf{M}\mathbf{x} = \mathbf{b}$ 
/* Initial Lanczos step */
 $\mathbf{u} \leftarrow \mathbf{M}\mathbf{x}$ ;  $\mathbf{w} \leftarrow \mathbf{b} - \mathbf{u}$ ;  $\beta_0 \leftarrow \|\mathbf{w}\|$ ;  $\mathbf{w} \leftarrow \mathbf{w}/\beta_0$ ;
 $\mathbf{u} \leftarrow \mathbf{M}\mathbf{w}$ ;  $\alpha \leftarrow \langle \mathbf{w}, \mathbf{u} \rangle$ ;  $\mathbf{u} \leftarrow \mathbf{u} - \alpha \cdot \mathbf{w}$ ;
/* Initial variables */
 $\beta_1 \leftarrow \beta_0$ ;  $\beta_2 \leftarrow \|\mathbf{u}\|$ ;
 $LQ_{\|\cdot\|} \leftarrow \beta_1$ ;  $CG_{\|\cdot\|} \leftarrow \beta_1$ ;  $QR_{\|\cdot\|} \leftarrow \beta_1$ ;  $r_{1,\|\cdot\|}^L \leftarrow \beta_1$ ;
 $\bar{\gamma} \leftarrow \alpha$ ;  $\bar{\delta} \leftarrow \beta_2$ ;  $r_{2,\|\cdot\|}^L \leftarrow 0$ ;  $S \leftarrow 1$ ;
 $\bar{T}_{\|\cdot\|_F^2} \leftarrow \alpha^2 + \beta_2^2$ ;  $z_{\|\cdot\|_F^2} \leftarrow 0$ ;  $\bar{\mathbf{w}} \leftarrow \mathbf{0}$ ;
while True do
   $d \leftarrow \bar{\gamma}$ ;
  /* Errors and stopping criterion */
  if  $d = 0$  then
     $d \leftarrow \sqrt{\bar{T}_{\|\cdot\|_F^2}}$ ;
   $LQ_{\|\cdot\|} \leftarrow \sqrt{(r_{1,\|\cdot\|}^L)^2 + (r_{2,\|\cdot\|}^L)^2}$ ;
   $QR_{\|\cdot\|} \leftarrow \beta_0 \cdot S$ ;
   $CG_{\|\cdot\|} \leftarrow (\beta_2 \cdot QR_{\|\cdot\|})/|d|$ ;
   $\bar{\zeta} \leftarrow r_{1,\|\cdot\|}^L/d$ ;
  if  $CG_{\|\cdot\|}^2 \leq \bar{T}_{\|\cdot\|_F^2} \cdot z_{\|\cdot\|_F^2} \cdot \epsilon^2$  then
    break;
  /* Lanczos step */
   $\mathbf{u} \leftarrow \mathbf{u}/\beta_2$ ;  $\mathbf{v} \leftarrow \mathbf{M}\mathbf{u}$ ;  $\alpha \leftarrow \langle \mathbf{u}, \mathbf{v} \rangle$ ;
   $\mathbf{v} \leftarrow \mathbf{v} - \alpha \cdot \mathbf{u} - \beta_2 \cdot \mathbf{w}$ ;  $\beta_1 \leftarrow \beta_2$ ;  $\beta_2 \leftarrow \|\mathbf{v}\|$ ;
  /* Update  $\bar{T}_{\|\cdot\|_F^2}$  norm */
   $\bar{T}_{\|\cdot\|_F^2} \leftarrow \bar{T}_{\|\cdot\|_F^2} + \alpha^2 + \beta_1^2 + \beta_2^2$ ;
  /* Next plane rotation */
   $\gamma \leftarrow \sqrt{\bar{\gamma}^2 + \beta_1^2}$ ;  $cs \leftarrow \bar{\gamma}/\gamma$ ;  $sn \leftarrow \beta_1/\gamma$ ;
   $\delta \leftarrow cs \cdot \bar{\delta} + sn \cdot \alpha$ ;  $\bar{\gamma} \leftarrow sn \cdot \bar{\delta} - cs \cdot \alpha$ ;  $\bar{\delta} \leftarrow -cs \cdot \beta_2$ ;
  /* Update  $\mathbf{x}$  and  $\bar{\mathbf{w}}$  */
   $\zeta \leftarrow r_{1,\|\cdot\|}^L/\gamma$ ;  $s \leftarrow cs \cdot \zeta$ ;  $t \leftarrow sn \cdot \zeta$ ;
   $\mathbf{x} \leftarrow \mathbf{x} + s \cdot \bar{\mathbf{w}} + t \cdot \mathbf{u}$ ;  $\bar{\mathbf{w}} \leftarrow sn \cdot \bar{\mathbf{w}} - cs \cdot \mathbf{u}$ ;
  /* Update variables */
   $S \leftarrow sn \cdot S$ ;  $z_{\|\cdot\|_F^2} \leftarrow z_{\|\cdot\|_F^2} + \zeta^2$ ;
   $r_{1,\|\cdot\|}^L \leftarrow r_{2,\|\cdot\|}^L - \delta \cdot \zeta$ ;  $r_{2,\|\cdot\|}^L \leftarrow -sn \cdot \beta_2 \cdot \zeta$ ;
  /* Cycle pointers for next iter. */
   $\mathbf{u} \leftarrow \mathbf{v} \leftarrow \mathbf{w} \leftarrow \mathbf{u}$ ;
/* Transfer to CG point */
if  $CG_{\|\cdot\|} \leq LQ_{\|\cdot\|}$  then
   $\bar{\zeta} \leftarrow r_{1,\|\cdot\|}^L/d$ ;  $\mathbf{x} \leftarrow \mathbf{x} + \bar{\zeta} \cdot \bar{\mathbf{w}}$ ;

```

---